

A study of dark matter-dark energy interaction under the DESI DR2 data constraint

Amin Aboubrahim^a and Pran Nath^{b,*}

^a*Department of Physics, University of Hartford,
200 Bloomfield Avenue, West Hartford, CT 06117, U.S.A.*

^b*Department of Physics, Northeastern University,
111 Forsyth Street, Boston, MA 02115-5000, U.S.A.*

E-mail: abouibrah@hartford.edu, p.nath@northeastern.edu

While Λ CDM provides a good fit to cosmological data, it fails to address many of the outstanding questions in contemporary cosmology. Chief among these are the Hubble tension and the apparent dynamical nature of dark energy as inferred from the recent DESI DR2 analysis. In this work, we analyze a field-theoretic description of cosmology where both dark energy and dark matter are interacting spin zero fields. We give a thorough study of a wide range of the interaction strength and demonstrate the effect on the dark energy equation of state and the Hubble tension. Using the recent cosmological data, we extract constraints on cosmological parameters including the free parameters of the model.

Proceedings of the Corfu Summer Institute 2025 "Tensions in Cosmology 2025 Conference" (CORFU2025)
September 2–8, 2025
Corfu, Greece

*Speaker

1. Introduction

The standard Λ CDM model successfully explains much cosmological data, but several tensions have emerged, most notably in the evaluation of the Hubble constant H_0 (for a recent review, see ref. [1] and references therein). A common approach which may provide a solution is to model dark matter-dark energy (DM-DE) interactions through source terms in the continuity equations, but these prescriptions are not derived from a consistent field-theoretic framework. Additional discrepancies have also appeared in measurements of the dark energy equation of state (EoS). Recent DESI results [2, 3] favor a time-varying EoS, which deviates from the Λ CDM prediction of $w = -1$. Quintessence models (particularly thawing and freezing types) provide alternative frameworks for generating such dynamical behavior without invoking the CPL parameterization [4, 5] which leads to phantom crossing.

This note is based on ref. [6] which examined whether a field-theoretic model of cosmology with DM-DE interaction can produce a dynamical EoS in agreement with DESI DR2, along with addressing the H_0 tension. The analysis avoids phenomenological continuity equations and instead uses a fully field-theoretic formulation that enforces energy conservation automatically. Within this framework, DM-DE coupling leads to rich EoS behavior: strong coupling can transform quintessence from thawing to scaling freezing, while weak coupling preserves the thawing regime. By fitting the EoS in both cases, the study evaluates how DM-DE interaction affects consistency with DESI DR2 data and finds that the couplings influence the results, although the DESI DR2 data points to a weak DM-DE interaction.

2. A model of cosmology with n interacting fields

We give a brief overview of the theory comprising of n interacting spin zero fields, ϕ_i , in the context of cosmology. This represents a generalization of the two-field case [7, 8]. The action of this theory, which we call QCDEM, is given by

$$S_{\text{QCDEM}} = \int d^4x \sqrt{-g} \left[\frac{1}{16\pi G} R + \sum_i \frac{1}{2} \phi_i^\mu \phi_{i,\mu} - V(\{\phi_i\}, \{\phi_j\}) \right], \quad (1)$$

where the potential is

$$V = \sum_i^n V_i(\phi_i) + V_{\text{int}}(\{\phi_i\}, \{\phi_j\}), \quad (2)$$

$$V_{\text{int}}(\{\phi_i\}, \{\phi_j\}) = \frac{1}{2} \sum_{i \neq j} \sum_j V_{ij}(\phi_i, \phi_j). \quad (3)$$

The quantity $V_{ij}(\phi_i, \phi_j)$ is the interaction potential between the fields ϕ_i and ϕ_j . The Klein-Gordon equation for the field ϕ_i is given by

$$\phi_i'' + 2\mathcal{H}\phi_i' + a^2 \left(V_{i,\phi_i} + \frac{1}{2} \sum_{j \neq i} (V_{ij} + V_{ji}), \phi_i \right) = 0, \quad (4)$$

where $V_{ij,\phi_i} \equiv \partial_{\phi_i} V_{ij}$, and $\mathcal{H} = a'/a$ is the conformal Hubble parameter. With the assumption $V_{ji} = V_{ij}$, the corresponding continuity equations are then given by

$$\rho'_i + 3\mathcal{H}(1 + w_i)\rho_i = Q_i, \quad (5)$$

$$Q_i = \sum_{j \neq i} V_{ij,\phi_j}(\phi_i, \phi_j) \phi'_j, \quad (6)$$

where $\sum_i Q_i \neq 0$ and the imposition of $\sum_i Q_i = 0$ implies $Q_i = 0$, i.e., no interaction at all. Further, the energy density ρ_i and the pressure p_i for the energy density of field ϕ_i are given by

$$\rho_i(p_i) = T_i \pm V_i(\phi_i) \pm \sum_{j \neq i} V_{ij}(\phi_i, \phi_j), \quad (7)$$

where T_i is the kinetic energy of field ϕ_i , the $+(-)$ signs are for the cases ρ_i (p_i), and $w_i = p_i/\rho_i$ is the equation of state. The total energy density is then defined by

$$\rho = \sum_i \rho_i - \sum_{i < j} V_{ij}(\phi_i, \phi_j), \quad (8)$$

where the last term on the right hand side is included to ensure no double counting. The observed relic density for the particle i is given by

$$\Omega_{0i} = \frac{\rho_i}{\rho_{0,\text{crit}}} (1 - \epsilon_i), \quad \sum_i \Omega_{0i} = 1, \quad \epsilon_i = \frac{\sum_{j \neq i} V_{ij}}{\sum_j \rho_j}. \quad (9)$$

Eq. (5) represents a consistent set of continuity equations for the case of n number of interacting fields, where the energy density ρ_i corresponds to the field ϕ_i .

3. Background and perturbation equations of QCMD

In this section, we summarize the evolution of DM and DE fields in a flat FLRW universe. In the interacting quintessence-DM (QCMD) framework, the DM field χ and DE field ϕ evolve under the potentials

$$V_1(\chi) = \frac{1}{2}m_\chi^2 \chi^2, \quad (10)$$

$$V_2(\phi) = \mu^4 \left[1 + \cos \left(\frac{\phi}{F} \right) \right], \quad (11)$$

and interact through

$$V_{\text{int}}(\phi, \chi) = \frac{\lambda}{2} \chi^2 \phi^2. \quad (12)$$

Perturbations are introduced as $\chi \rightarrow \chi + \chi_1$ and $\phi \rightarrow \phi + \phi_1$, with the synchronous gauge line element $ds^2 = a^2(\tau) [-d\tau^2 + (\delta_{ij} + h_{ij}) dx^i dx^j]$.

The background fields satisfy the Klein-Gordon equations

$$\chi'' + 2\mathcal{H}\chi' + a^2(V_{1,\chi} + V_{12,\chi}) = 0, \quad (13)$$

$$\phi'' + 2\mathcal{H}\phi' + a^2(V_{2,\phi} + V_{12,\phi}) = 0. \quad (14)$$

Because the DM field oscillates rapidly when $\mathcal{H}/m_\chi \ll 1$ [9, 10], it is convenient to redefine the DM energy density as $\tilde{\rho}_\chi = \rho_\chi - V_{12}$ and introduce the modified fraction

$$\tilde{\Omega}_\chi = \frac{\kappa^2}{6\mathcal{H}^2} \left(\chi_0'^2 + 2a^2 V_1(\chi_0) \right), \quad (15)$$

along with new dimensionless variables [11, 12]

$$\tilde{\Omega}_\chi^{1/2} \sin\left(\frac{\theta}{2}\right) = \frac{\kappa\chi'}{\sqrt{6}\mathcal{H}}, \quad (16)$$

$$\tilde{\Omega}_\chi^{1/2} \cos\left(\frac{\theta}{2}\right) = \frac{\kappa a V_1^{1/2}}{\sqrt{3}\mathcal{H}}, \quad (17)$$

$$y = -\frac{2\sqrt{2}a}{\mathcal{H}} \partial_\chi V_1^{1/2}. \quad (18)$$

These variables absorb the rapid oscillations into θ , allowing the DM KG equation to be rewritten as three first-order differential equations:

$$\Omega_\chi' = 3\mathcal{H}\Omega_\chi(w_T - w_\chi) + \frac{\kappa^2 a^2}{3\mathcal{H}^2} \left[\mathcal{H}(1 + 3w_\chi)V_{12} - \chi' V_{12,\chi} \right], \quad (19)$$

$$\theta' = -3\mathcal{H} \sin \theta + \mathcal{H}y - \frac{\kappa^2 a^2}{3\mathcal{H}^2 \tilde{\Omega}_\chi} \left(2\mathcal{H}V_{12} + \chi' V_{12,\chi} \right) \cot \frac{\theta}{2}, \quad (20)$$

$$y' = \frac{3}{2}\mathcal{H}(1 + w_T)y. \quad (21)$$

In this parametrization, the DM equation of state becomes $w_\chi = -\cos \theta$, which oscillates between $+1$ and -1 , yielding a vanishing time average, consistent with CDM. The interaction term is omitted from $\tilde{\rho}_\chi$ and $\tilde{\rho}_\chi$ but reappears in the evolution equations.

Linear perturbations obey the KG equations

$$\phi_1'' + 2\mathcal{H}\phi_1' + (k^2 + a^2 V_{,\phi\phi})\phi_1 + a^2 V_{,\phi\chi}\chi_1 + \frac{1}{2}h'\phi' = 0, \quad (22)$$

$$\chi_1'' + 2\mathcal{H}\chi_1' + (k^2 + a^2 V_{,\chi\chi})\chi_1 + a^2 V_{,\chi\phi}\phi_1 + \frac{1}{2}h'\chi' = 0, \quad (23)$$

leading to energy density and pressure perturbations

$$\delta\rho_\phi = \frac{1}{a^2} \phi'\phi_1' + (V_2 + V_{12})_{,\phi}\phi_1 + V_{12,\chi}\chi_1, \quad (24)$$

$$\delta p_\phi = \frac{1}{a^2} \phi'\phi_1' - (V_2 + V_{12})_{,\phi}\phi_1 - V_{12,\chi}\chi_1, \quad (25)$$

$$\delta\rho_\chi = \frac{1}{a^2} \chi'\chi_1' + (V_1 + V_{12})_{,\chi}\chi_1 + V_{12,\phi}\phi_1, \quad (26)$$

$$\delta p_\chi = \frac{1}{a^2} \chi'\chi_1' - (V_1 + V_{12})_{,\chi}\chi_1 - V_{12,\phi}\phi_1. \quad (27)$$

The velocity divergences, $\Theta = ik^i v_i$, are

$$(\rho_\phi + p_\phi)\Theta_\phi = \frac{k^2}{a^2} \phi'\phi_1, \quad (28)$$

$$(\rho_\chi + p_\chi)\Theta_\chi = \frac{k^2}{a^2} \chi'\chi_1, \quad (29)$$

and the density contrast is defined as $\delta = \delta\rho/\rho$.

4. Phenomenological study of QCDM

The model is implemented in the Boltzmann equation solver **CLASS** [13] which evolves the background and perturbation equations from $a_{\text{ini}} = 10^{-14}$ to $a_0 = 1$ (today). The input parameters of the model are $\mu^4, F, \lambda, \phi_{\text{ini}}, \phi'_{\text{ini}}, \chi_{\text{ini}}, \chi'_{\text{ini}}$. The DE field velocity is chosen as $\phi'_{\text{ini}} = 10^{-3}$ and an estimate of μ^4 is determined by minimizing the DE potential so that $\mu^4 = \frac{3}{2} H_0^2 \Omega_{\phi 0}$, where $\Omega_{\phi 0}$ is today's DE density fraction. This value serves as an initial estimate and we modify μ^4 accordingly in order to achieve a consistent cosmology.

Depending on the size of λ , we can distinguish between two regimes: the strong coupling regime and the weak coupling regime. Figure 1 shows the evolution of DM (dotted line) and DE (solid line) equations of state as a function of the redshift $1+z$ for the strong coupling regime, where we have set $\lambda = 10 m_{\text{pl}}^{-2} \text{Mpc}^{-2}$. Examining the left panel: initially $w_\chi = -1$ and $w_\phi = +1$, so χ behaves as an early DE component while ϕ acts as radiation. Rapid oscillations in χ begin near $z \sim 10^5$, and their averaging yields $w_\chi = 0$, causing $\rho_\chi \propto a^{-3}$ as for CDM. The field ϕ transitions from radiation-like behavior to $w_\phi \rightarrow -1$ as its potential rolls to the minimum and later begins oscillating around $z \sim 10^2$. Unlike χ , whose oscillation amplitude is constant, the ϕ oscillations decay. For $\phi/F \ll 1$, Eq. (14) becomes

$$\phi'' + 2\mathcal{H}\phi' + a^2 m_\phi^2 \phi \approx 0, \quad (30)$$

with $m_\phi^2 = \lambda \chi^2 - \mu^4/F^2$. When λ is large enough for $m_\phi^2 > 0$, oscillations begin once $\mathcal{H}/m_\phi \ll 1$.

Averaging these oscillations, the right panel of Fig. 1 shows w_ϕ deviating from and then returning toward -1 . For $\phi_{\text{ini}} = 0.1$, w_ϕ evolves to -1 as expected; for $\phi_{\text{ini}} = 0.5$, it approaches $w_\phi \sim -0.9$; and for $\phi_{\text{ini}} = 1.0$, oscillations persist till $z = 0$, giving an average EoS far from -1 , making this value of ϕ_{ini} observationally disfavored.

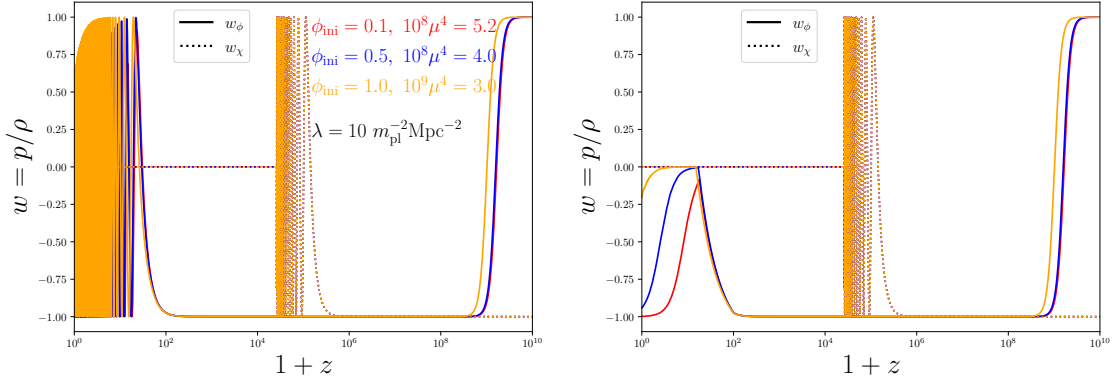


Figure 1: Plot of the evolution of the equations of state (EoS) of DM and DE (left) and a time-average over the oscillations in w_ϕ (right panel). The DM EoS, w_χ , is being averaged over in both panels after a short period of oscillations. The color code correspond to different values of ϕ_{ini} and μ^4 in the presence of DM-DE interaction, expressed in standard **CLASS** units of m_{pl} and $m_{\text{pl}}^2/\text{Mpc}^2$, respectively. Figure is adapted from ref. [6].

Figure 2 illustrates the late-time behavior of the DE equation of state, focusing on the peculiar evolution of w_ϕ for $z < 10^2$. The solid curves show the QCDM predictions for five values of the

interaction strength λ , while the dashed curves represent the fit

$$w(a) = -1 + \frac{\alpha a^p e^{-p a}}{1 + (\beta a)^q}, \quad (31)$$

with α , β , p , and q as free parameters. For these benchmarks, w_ϕ departs from -1 in the range $10 < z < 100$, initially following a thawing-quintessence behavior before turning around and returning toward -1 at late times, similar to scaling freezing. Thus, the DM-DE interaction induces a transition of the DE from thawing to scaling freezing, a behavior disfavored by recent DESI constraints.

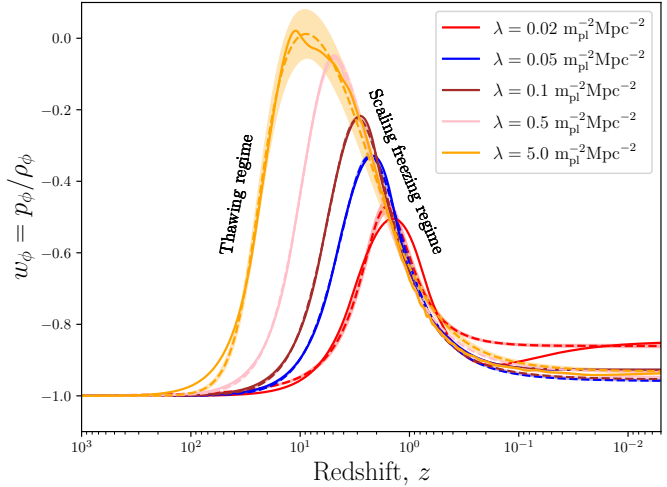


Figure 2: The evolution of w_ϕ as a function of the redshift z is shown for five choices of the interaction strength λ . The solid curves display the QCDM predictions, while the dashed curves provide fits using Eq. (31) together with the corresponding 1σ uncertainty bands. For all parameter choices, the DE equation of state exhibits a transition induced by λ , evolving from a thawing behavior at higher redshift to a scaling-freezing behavior at lower redshift. Figure is adapted from ref. [6].

To assess this, Fig. 3 compares two cases: no interaction (dashed curves) and a non-zero interaction (solid curves). The evolution of w_ϕ over $0.1 < a < 1$ is shown along with the DESI+CMB+PantheonPlus 1σ bounds for the w CDM model with constant w (green band) and the CPL form $w(a) = w_0 + (1 - a)w_a$ known as the w_0w_a CDM model (blue band). Without interaction, the EoS stays near -1 until $a \sim 0.3$, consistent with thawing PNGB potentials [14]. One benchmark agrees with DESI's w CDM constraints¹, while others deviate significantly and align with w_0w_a CDM near $a = 1$.

When the DM-DE interaction is included, the EoS qualitatively changes: w_ϕ evolves toward -1 in a manner characteristic of scaling freezing models [11, 20]. The interaction effectively reshapes the DE potential so that the resulting behavior resembles that of a double-exponential form, $V_S(\phi) = \tilde{V}_0(e^{-\lambda_1\phi} + e^{-\lambda_2\phi})$. Both thawing and scaling-freezing regimes for w_ϕ are visible in the right panel of Fig. 1, with a transition occurring near $z_t \sim 10$ when $\lambda \neq 0$.

¹See recent analyses in Refs. [15–19].

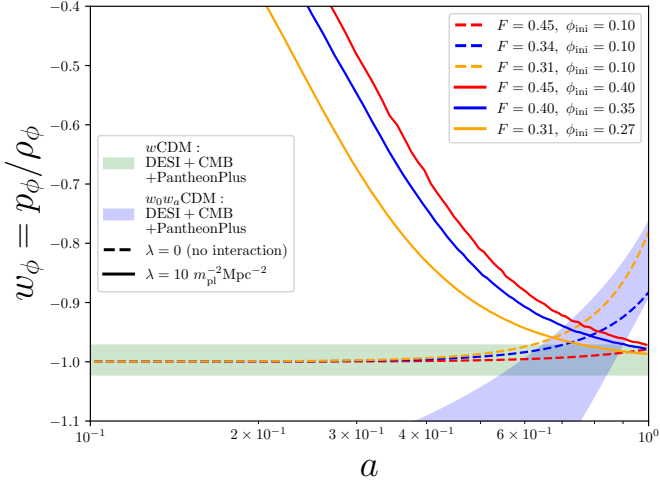


Figure 3: The evolution of the DE equation of state in the narrow interval $0.1 < a < 1$ for the case of no interaction (dashed curves) and the case of DM-DE interaction (solid curves). The colors of each curve correspond to a choice of (F, ϕ_{ini}) as indicated in the figure legend. Both F and ϕ_{ini} are in units of m_{pl} . The blue and green bands are the 1σ regions from DESI’s interpretations of their data based on the w_0w_a CDM and w CDM models, respectively. Figure is adapted from ref. [6].

Using DESI DR1 and DR2 constraints, a quintessence model exhibiting a freezing behavior is incompatible with the allowed ranges of w_0 and w_a . Although our framework contains several free parameters ($F, \phi_{\text{ini}}, \mu^4$, and λ), we verified that no parameter choice in the strong coupling regime can reproduce the DESI preferred values. Expanding Eq. (31) around $\epsilon = (1 - a)$ to linear order yields

$$w_0 = -1 + \frac{\alpha e^{-p}}{1 + \beta^q}, \quad (32)$$

$$w_a = \frac{q \beta^q}{1 + \beta^q} (1 + w_0), \quad (33)$$

showing that DESI effectively fixes two of the four parameters in Eq. (31). For instance, one may use measured w_0 and w_a to solve Eq. (33) for β^q and Eq. (32) for e^{-p} , leaving α and q free. Using these remaining parameters, we attempted to fit the model predictions but found no viable fit in the strong coupling regime. As anticipated, current DESI data does not support quintessence models with a scaling-freezing equation of state. Therefore, the strong coupling regime is not favored.

Next, we examine the weak coupling regime, i.e., $\lambda \leq 10^{-2}$. We find that in this regime, the dark energy EoS can be fitted by the function

$$\hat{w}(a) = -1 + \alpha e^{-\beta a} \arctan(p a^q), \quad (34)$$

with α, β, p and q being the fit parameters. Expanding Eq. (34) up to first order in $(1 - a)$, we get w_0 and w_a so that

$$w_0 = -1 + \alpha e^\beta \arctan(p), \quad (35)$$

$$w_a = \frac{\alpha e^{-\beta}}{1 + p^2} \left[-p q + \beta(1 + p^2) \arctan(p) \right]. \quad (36)$$

We fit the DE equation of state, $w_\phi(a)$, obtained from our model to the parametrization $\hat{w}(a) = w_0 + (1 - a)w_a$ and extract the corresponding values of w_0 and w_a for each model data point. Among all points, we retain the ones that minimize the χ^2 statistic,

$$\chi^2 = \sum_i \left(\frac{w_i(a) - \hat{w}_i(a)}{\sigma_i} \right)^2, \quad (37)$$

which identifies the best-fit model.

Our model contains four input parameters, and to identify which of them most strongly drives the values of w_0 and w_a toward the DESI-preferred 2σ region, we employ SHAP (SHapley Additive exPlanations) [21]. We train a gradient-boosted decision tree classifier (XGBClassifier) using the XGBoost framework [22] on the Monte Carlo samples generated from our model that represent the best-fit model points. The classifier learns how combinations of input parameters lead to points that lie within the 2σ constraints on (w_0, w_a) .

XGBoost produces an ensemble of decision trees that assign probabilities indicating whether a given point satisfies the observational bounds. These probabilities are then analyzed with TreeSHAP, a fast algorithm within SHAP that computes exact Shapley values. Treating each model parameter as a feature, the resulting SHAP values quantify the contribution of each feature to the model outcome, allowing us to determine which parameter most significantly influences whether the predicted (w_0, w_a) fall within DESI limits. Using this techniques, we derive an upper limit on the DM-DE interaction strength, λ , for each data set. We find that for DESI + CMB + PantheonPlus, $\log \lambda < -2.78$, for DESI + CMB + Union3, $\log \lambda < -2.99$ and for DESI + CMB + DESY5, $\log \lambda < -3.26$. So, the PantheonPlus data set imposes the strongest upper limit on the interaction strength.

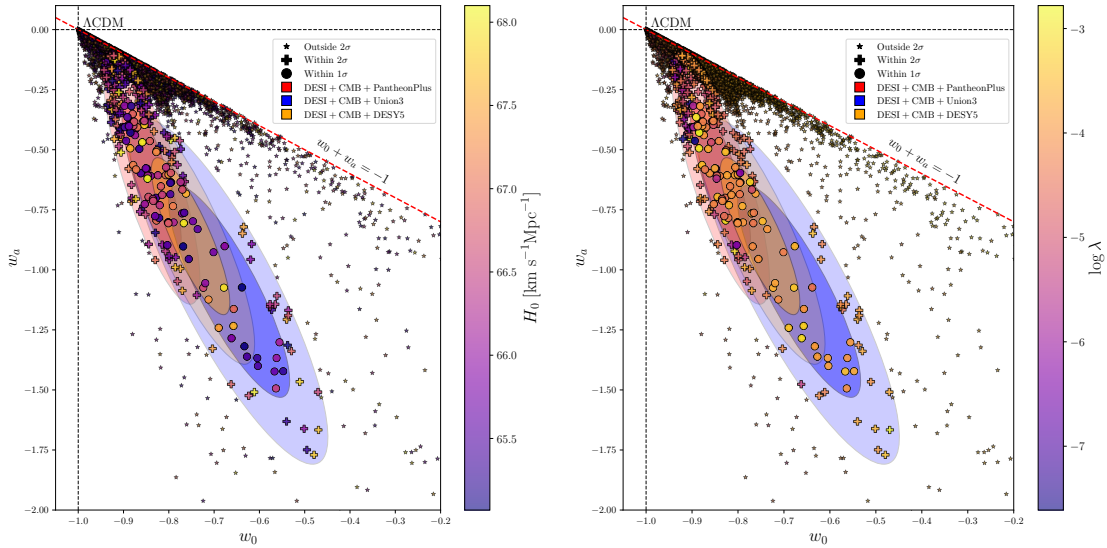


Figure 4: Scatter plots in the w_0 - w_a plane are shown overlaid on the DESI DR2 posterior contours with the upper bound on $\log \lambda$ imposed for each data set. The left panel uses the Hubble parameter H_0 as the color scale, while the right panel displays $\log \lambda$. The model yields parameter points that fall within the 1σ and 2σ posterior regions of the considered data sets. Figure is adapted from ref. [6].

Figure 4 displays the model points that satisfy the imposed upper bound on λ as well as the constraints on H_0 and Ω_m . Even with λ values approaching the upper limit, a substantial number of points continue to fall within the 1σ and 2σ posterior regions of DESI's data set combination in the w_0 - w_a plane.

5. Extraction of cosmological parameters with MCMC and Bayesian inference

Because a DM-DE interaction affects not only the background evolution but also density perturbations (and hence the CMB temperature/polarization spectra and the matter power spectrum), we confront the model with current cosmological data: Planck 2018 CMB measurements, DESI-DR2 BAO, and several SN-based local distance data sets. We implement the model in CLASS by evolving the background equations together with the synchronous-gauge KG perturbation equations for the fields ϕ and χ , namely Eqs. (22) and (23), while all other species follow their standard Λ CDM evolution. We set $\chi_1 = \chi'_1 = 0$ and $\phi_1 = \phi'_1 = 0$ initially (analogous to $\delta_{\text{ini}} = 0$ and $\Theta_{\text{ini}} = 0$), noting that the perturbations are rapidly driven to the attractor solution [23]. Since the synchronous gauge is not fully fixed by a scalar-field DM component (because w_χ is dynamical rather than identically zero), we retain the use of synchronous gauge in CLASS by including a small CDM component, $\Omega_{\text{CDM}} h^2 = 10^{-5}$.

We use the following likelihoods and data sets: **CMB** (Planck TT, TE, EE, low- ℓ , and lensing) [24–27], **DESI DR2** (BAO measurements) [3, 28], **PPS** (PantheonPlus+SH0ES) [29, 30], **Union3** (2087 SN Ia) [31], and **DESY5** (DES Year 5 SN sample) [32].

For inference, we interface CLASS with Cobaya [33] to perform MCMC sampling (adaptive, speed-hierarchy-aware sampler adapted from CosmoMC) [34, 35] using fast-dragging [36]. Convergence is assessed with the Gelman-Rubin criterion $R - 1 < 0.05$ [37], and posterior constraints are extracted with GetDist [38]. The sampled parameters include the six Λ CDM parameters plus $\log \mu^4$, F , ϕ_{ini} , and $\log \lambda$, all with flat priors.

Including perturbations, the results (Table 1) provide 68% CL constraints for multiple data combinations. The baryon density fraction remains nearly unchanged across combinations, while the inferred DM fraction increases by more than $\sim 5\%$ when SN data such as DESY5 and Union3 are included relative to the first two combinations. The model parameter μ^4 is constrained to values of order $10^{-8} \text{ m}_{\text{Pl}}^2/\text{Mpc}^2$ (e.g. from $\sim 5.5 \times 10^{-8}$ for CMB+DESI up to $\sim 7.6 \times 10^{-8}$ for CMB+DESI+Union3). The tightest lower bound on F arises from CMB+DESI+PPS (e.g. $F > 0.62$), while it relaxes with DESY5 inclusion (down to $F \sim 0.29$). An upper bound on ϕ_{ini} is obtained, with PPS giving the most stringent limit. All data combinations favor weak coupling, yielding upper limits in the range $\lambda \lesssim 10^{-3}$ down to $\lambda \lesssim 10^{-5.7}$, which are stronger than constraints obtained from background evolution alone. The model only modestly alleviates the Hubble tension at 95% CL (largest shifts driven by PPS). For structure growth, the derived $S_8 \equiv \sigma_8 \sqrt{\Omega_m/0.3}$ is consistent with recent KiDS-Legacy results [39]. Finally, using Eqs. (35) and (36) with DESI DR2, the inferred values remain close to Λ CDM, $w_0 \simeq -1$ and $w_a \simeq 0$, although the SN data (notably DESY5 and Union3) significantly shifts the preferred (w_0, w_a) and enlarges evidence for mild evolution.

Parameter	CMB+DESI	CMB+DESI+PPS	CMB+DESI+DESY5	CMB+DESI+Union3
$\log(10^{10} A_s)$	3.042 ± 0.010	3.046 ± 0.013	3.044 ± 0.011	3.045 ± 0.012
n_s	0.9684 ± 0.0036	0.9703 ± 0.0033	0.9696 ± 0.0037	0.9694 ± 0.0035
$100\theta_s$	1.04217 ± 0.00029	1.04227 ± 0.00027	1.04219 ± 0.00028	1.04220 ± 0.00028
$\Omega_b h^2$	0.02278 ± 0.00011	0.02283 ± 0.00011	0.02278 ± 0.00011	0.02279 ± 0.00011
Ω_χ	0.2420 ± 0.0083	0.2415 ± 0.0066	$0.256^{+0.011}_{-0.0097}$	$0.2543^{+0.0093}_{-0.012}$
z_{reio}	7.69 ± 0.48	7.86 ± 0.61	7.80 ± 0.56	7.84 ± 0.60
$\log \mu^4$	$-7.233^{+0.013}_{-0.028}$	$-7.230^{+0.013}_{-0.024}$	$-7.192^{+0.041}_{-0.065}$	$-7.175^{+0.053}_{-0.075}$
$F [m_{\text{Pl}}]$	> 0.561	> 0.620	$0.51^{+0.20}_{-0.22}$	$0.63^{+0.23}_{-0.17}$
$\phi_{\text{ini}} [m_{\text{Pl}}]$	< 0.157	< 0.263	< 0.384	< 0.560
$\log \lambda$	$-4.9^{+2.0}_{-2.7}$	$-5.49^{+0.97}_{-2.2}$	< -5.49	< -5.69
<hr/>				
$H_0 [\text{km/s/Mpc}]$	$69.4^{+1.1}_{-0.98}$	69.39 ± 0.87	$67.6^{+1.3}_{-1.6}$	$67.8^{+1.6}_{-1.3}$
Ω_m	$0.276^{+0.029}_{-0.016}$	$0.280^{+0.025}_{-0.011}$	$0.294^{+0.028}_{-0.015}$	$0.295^{+0.024}_{-0.015}$
Ω_ϕ	0.7092 ± 0.0097	$0.7097^{+0.0079}_{-0.0071}$	0.693 ± 0.012	$0.695^{+0.014}_{-0.011}$
τ_{reio}	0.0559 ± 0.0049	$0.0579^{+0.0060}_{-0.0068}$	$0.0571^{+0.0054}_{-0.0061}$	0.0575 ± 0.0062
S_8	$0.769^{+0.034}_{-0.018}$	$0.773^{+0.028}_{-0.014}$	$0.778^{+0.027}_{-0.014}$	$0.780^{+0.023}_{-0.012}$
w_0	$-0.900^{+0.069}_{-0.25}$	$-0.937^{+0.021}_{-0.17}$	$-0.925^{+0.055}_{-0.13}$	$-0.890^{+0.075}_{-0.16}$
w_a	$-0.018^{+0.035}_{-0.016}$	$-0.018^{+0.029}_{-0.013}$	$-0.076^{+0.11}_{-0.046}$	$-0.109^{+0.14}_{-0.070}$
$\Delta\chi^2_{\text{min}}$	25.11	21.61	14.23	21.05
ΔAIC	33.11	29.61	22.23	29.05

Table 1: Constraints on some of the cosmological parameters of our model. The values are quoted at 68% CL intervals for three data set combinations. The middle double line separates the sampled and derived parameters using MCMC. In the last two rows we show the values of $\Delta\text{AIC} \equiv \text{AIC}_{\text{QCDM}} - \text{AIC}_{\Lambda\text{CDM}}$ and $\Delta\chi^2_{\text{min}} \equiv \chi^2_{\text{QCDM},\text{min}} - \chi^2_{\Lambda\text{CDM},\text{min}}$. Table is taken from ref. [6].

To compare QCDM against Λ CDM, we compute the Akaike Information Criterion (AIC) [40],

$$\text{AIC} \equiv -2 \ln \mathcal{L}_{\text{max}} + 2K, \quad (38)$$

and define $\Delta\text{AIC} \equiv \text{AIC}_{\text{QCDM}} - \text{AIC}_{\Lambda\text{CDM}}$. Using the usual rule of thumb ($\Delta\text{AIC} < -5$ favors QCDM, while $\Delta\text{AIC} > 10$ decisively favors Λ CDM), the results in Table 1 indicate $\Delta\text{AIC} > 10$ for all data combinations, i.e. the data prefer Λ CDM over the interacting QCDM model.

Figure 5 shows the correlation between H_0 and $\log \lambda$ (left) and between S_8 and $\log \lambda$ (right), with the gray bands indicating the 1σ and 2σ experimental ranges. The 1σ contours of H_0 for both data sets do not overlap with the measured value of H_0 , whereas the corresponding contours for S_8 lie within its experimental band. Thus, the QCDM model only mildly alleviates the H_0 tension, while S_8 shows no significant tension.

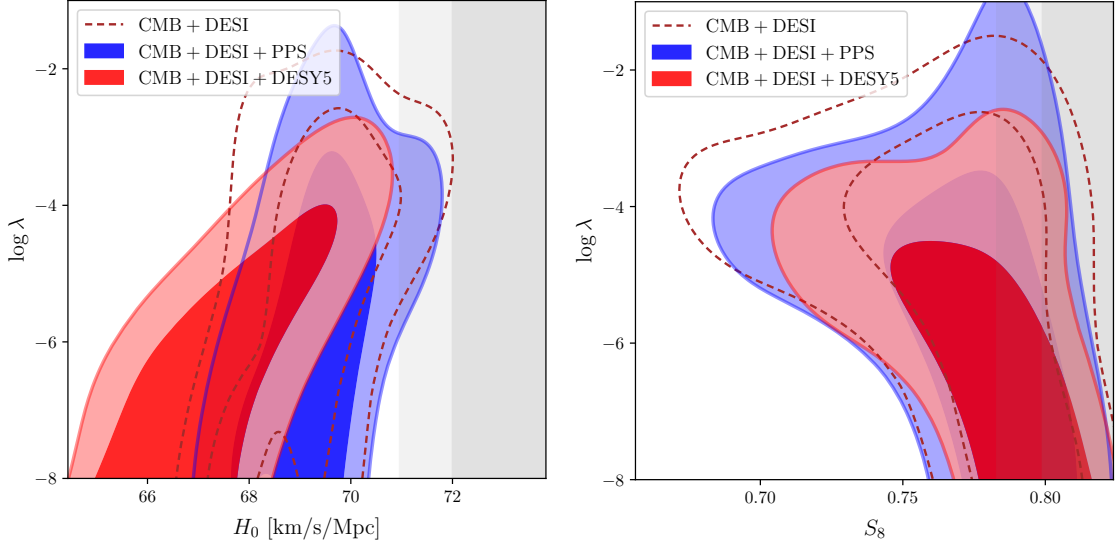


Figure 5: The two-dimensional marginalized contours at the 68% and 95% confidence levels are shown for the DM-DE coupling strength versus H_0 (left panel) and versus S_8 (right panel). In the left panel, the gray bands indicate the SH0ES [30] measurement, $H_0 = 73.04 \pm 1.04 \text{ km s}^{-1} \text{ Mpc}^{-1}$, while in the right panel they represent the KiDS-Legacy [39] constraint, $S_8 = 0.815^{+0.016}_{-0.021}$. Figure is adapted from ref. [6].

We now examine how the different data sets impact the inferred values of w_0 and w_a , and what this implies for evolving dark energy. The left panel of Fig. 6 shows the 1σ and 2σ contours in the w_0 - w_a plane for the four data set combinations. A substantial portion of the allowed region lies in the fourth quadrant ($w_0 < 0$, $w_a < 0$); however, unlike the DESI DR2 results, parts of the contours extend into other quadrants and overlap with the Λ CDM point $(w_0, w_a) = (-1, 0)$. Although the constraints remain consistent with $w_0 = -1$, the 1σ and 2σ regions still leave ample room for an evolving DE equation of state near $a = 1$. The best-fit points, marked by filled dots for each of the PPS, DESY5, and Union3 data sets, all fall in the fourth quadrant, thereby favoring evolution in the DE component.

In contrast to PantheonPlus+SH0ES, the DESY5 and Union3 samples push the preferred values of (w_0, w_a) toward an evolving DE scenario while staying within the quintessence regime (i.e., without crossing the phantom divide). It is important to emphasize that although we describe the DE EoS using the CPL form, w_0 and w_a are *derived* quantities in this model and depend on the underlying particle physics parameters rather than being freely varied. To highlight the difference from DESI's analysis, we overlay DESI's (unfilled) contours in the right panel of Fig. 6. These contours reach further into the fourth quadrant relative to our results, reflecting the phantom-divide crossing behavior that appears when CPL is treated as a purely phenomenological parametrization.

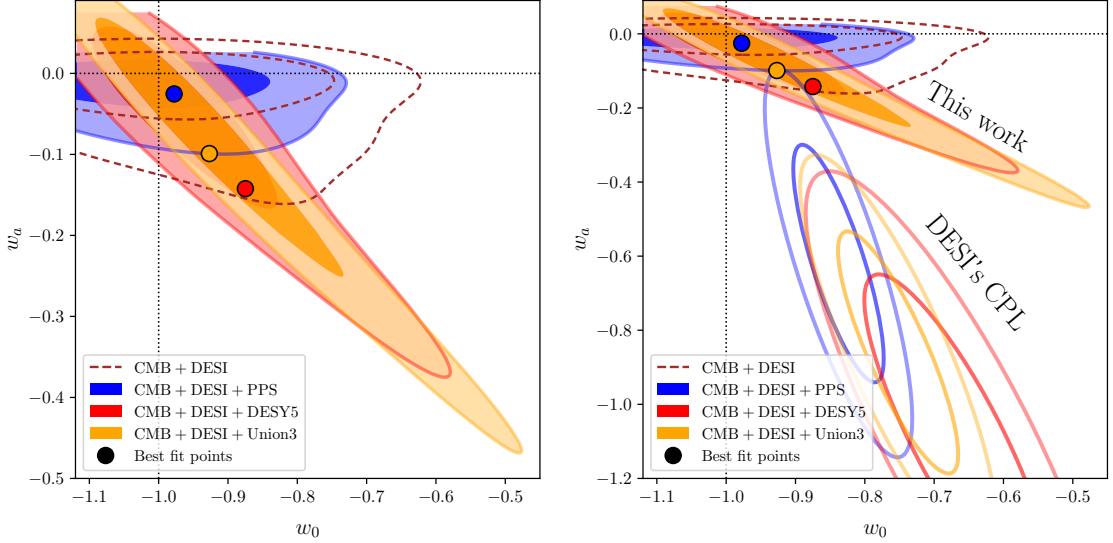


Figure 6: Left panel: Posterior contours for (w_0, w_a) obtained from the four data-set combinations: CMB+DESI (dashed), CMB+DESI+PPS (blue), CMB+DESI+DESY5 (red), and CMB+DESI+Union3 (orange). The dotted vertical and horizontal lines mark the Λ CDM point $(w_0, w_a) = (-1, 0)$. Filled dots indicate the best-fit values for the PPS, DESY5, and Union3 cases. Right panel: Same as the left panel, with DESI's unfilled contours added for comparison. Figure is adapted from ref. [6].

6. Conclusion

In this work, we investigated a field-theoretic cosmological model in which dark matter and dark energy are described by ultralight spin zero fields coupled through an explicit interaction term. Using a specific choice of dark energy potential together with the interaction term, we analyzed the resulting evolution of the dark energy equation of state.

Our study identifies two qualitatively distinct regimes: a strong-coupling region ($\lambda \geq 10^{-2}$) and a weak-coupling region ($\lambda < 10^{-2}$). In the strong-coupling regime, the DE equation of state undergoes a transmutation from thawing behavior at early times to scaling-freezing behavior at late times. Because a freezing DE equation of state today is disfavored by DESI, this regime is effectively ruled out. In contrast, the weak-coupling regime yields evolution consistent with DESI, supporting a mildly evolving DE component. We provided a fit for $w_\phi(a)$ which, to leading order in $(1-a)$, produces values of (w_0, w_a) compatible with DESI without requiring a phantom-divide crossing.

Using DESI data set combinations, we obtained an upper limit on λ and showed that many benchmark points near this limit remain viable. Incorporating cosmological perturbations allowed us to derive tighter constraints on the full parameter space. Overall, the results indicate that the QCDM framework accommodates a cosmological-constant-like behavior while still permitting an evolving DE equation of state. This is reflected in the best-fit points across all data sets, which fall in the fourth quadrant of the (w_0, w_a) plane, signaling a preference for evolving quintessence.

Acknowledgments

The research of PN was supported in part by the NSF Grant PHY-2209903. The analysis presented here was done using the computing resources of the Phage Cluster at Union College.

References

- [1] **CosmoVerse Network** Collaboration, E. Di Valentino et al., *The CosmoVerse White Paper: Addressing observational tensions in cosmology with systematics and fundamental physics*, *Phys. Dark Univ.* **49** (2025) 101965, [[arXiv:2504.01669](https://arxiv.org/abs/2504.01669)].
- [2] **DESI** Collaboration, A. G. Adame et al., *DESI 2024 VI: cosmological constraints from the measurements of baryon acoustic oscillations*, *JCAP* **02** (2025) 021, [[arXiv:2404.03002](https://arxiv.org/abs/2404.03002)].
- [3] **DESI** Collaboration, M. Abdul Karim et al., *DESI DR2 results. II. Measurements of baryon acoustic oscillations and cosmological constraints*, *Phys. Rev. D* **112** (2025), no. 8 083515, [[arXiv:2503.14738](https://arxiv.org/abs/2503.14738)].
- [4] M. Chevallier and D. Polarski, *Accelerating universes with scaling dark matter*, *Int. J. Mod. Phys. D* **10** (2001) 213–224, [[gr-qc/0009008](https://arxiv.org/abs/gr-qc/0009008)].
- [5] E. V. Linder, *Exploring the expansion history of the universe*, *Phys. Rev. Lett.* **90** (2003) 091301, [[astro-ph/0208512](https://arxiv.org/abs/astro-ph/0208512)].
- [6] A. Aboubrahim and P. Nath, *Upper limits on dark energy-dark matter interaction from DESI DR2 in a field-theoretic analysis*, *JCAP* **10** (2025) 081, [[arXiv:2411.11177](https://arxiv.org/abs/2411.11177)].
- [7] A. Aboubrahim and P. Nath, *Interacting ultralight dark matter and dark energy and fits to cosmological data in a field theory approach*, *JCAP* **09** (2024) 076, [[arXiv:2406.19284](https://arxiv.org/abs/2406.19284)].
- [8] P. Nath and A. Aboubrahim, *Cosmological tensions and $QCDM$ as an alternative to ΛCDM* , *PoS CORFU2024* (2025) 203, [[arXiv:2503.09769](https://arxiv.org/abs/2503.09769)].
- [9] M. S. Turner, *Coherent Scalar Field Oscillations in an Expanding Universe*, *Phys. Rev. D* **28** (1983) 1243.
- [10] L. A. Ureña-López and A. X. Gonzalez-Morales, *Towards accurate cosmological predictions for rapidly oscillating scalar fields as dark matter*, *JCAP* **07** (2016) 048, [[arXiv:1511.08195](https://arxiv.org/abs/1511.08195)].
- [11] E. J. Copeland, A. R. Liddle, and D. Wands, *Exponential potentials and cosmological scaling solutions*, *Phys. Rev. D* **57** (1998) 4686–4690, [[gr-qc/9711068](https://arxiv.org/abs/gr-qc/9711068)].
- [12] G. Garcia-Arroyo, L. A. Ureña-López, and J. A. Vázquez, *Interacting scalar fields: Dark matter and early dark energy*, *Phys. Rev. D* **110** (2024), no. 2 023529, [[arXiv:2402.08815](https://arxiv.org/abs/2402.08815)].
- [13] D. Blas, J. Lesgourgues, and T. Tram, *The Cosmic Linear Anisotropy Solving System (CLASS) II: Approximation schemes*, *JCAP* **07** (2011) 034, [[arXiv:1104.2933](https://arxiv.org/abs/1104.2933)].

- [14] J. A. Frieman, C. T. Hill, A. Stebbins, and I. Waga, *Cosmology with ultralight pseudo Nambu-Goldstone bosons*, *Phys. Rev. Lett.* **75** (1995) 2077–2080, [[astro-ph/9505060](#)].
- [15] Y. Tada and T. Terada, *Quintessential interpretation of the evolving dark energy in light of DESI observations*, *Phys. Rev. D* **109** (2024), no. 12 L121305, [[arXiv:2404.05722](#)].
- [16] J. Rebouças, D. H. F. de Souza, K. Zhong, V. Miranda, and R. Rosenfeld, *Investigating late-time dark energy and massive neutrinos in light of DESI Y1 BAO*, *JCAP* **02** (2025) 024, [[arXiv:2408.14628](#)].
- [17] K. V. Berghaus, J. A. Kable, and V. Miranda, *Quantifying scalar field dynamics with DESI 2024 Y1 BAO measurements*, *Phys. Rev. D* **110** (2024), no. 10 103524, [[arXiv:2404.14341](#)].
- [18] W. J. Wolf, P. G. Ferreira, and C. García-García, *Matching current observational constraints with nonminimally coupled dark energy*, *Phys. Rev. D* **111** (2025), no. 4 L041303, [[arXiv:2409.17019](#)].
- [19] I. D. Gialamas, G. Hütsi, K. Kannike, A. Racioppi, M. Raidal, M. Vasar, and H. Veermäe, *Interpreting DESI 2024 BAO: Late-time dynamical dark energy or a local effect?*, *Phys. Rev. D* **111** (2025), no. 4 043540, [[arXiv:2406.07533](#)].
- [20] P. G. Ferreira and M. Joyce, *Structure formation with a selftuning scalar field*, *Phys. Rev. Lett.* **79** (1997) 4740–4743, [[astro-ph/9707286](#)].
- [21] S. Lundberg and S.-I. Lee, *A Unified Approach to Interpreting Model Predictions*, [[arXiv:1705.07874](#)].
- [22] T. Chen and C. Guestrin, *XGBoost: A Scalable Tree Boosting System*, [[arXiv:1603.02754](#)].
- [23] G. Ballesteros and J. Lesgourgues, *Dark energy with non-adiabatic sound speed: initial conditions and detectability*, *JCAP* **10** (2010) 014, [[arXiv:1004.5509](#)].
- [24] **Planck** Collaboration, N. Aghanim et al., *Planck 2018 results. VI. Cosmological parameters*, *Astron. Astrophys.* **641** (2020) A6, [[arXiv:1807.06209](#)]. [Erratum: *Astron. Astrophys.* 652, C4 (2021)].
- [25] **Planck** Collaboration, N. Aghanim et al., *Planck 2018 results. I. Overview and the cosmological legacy of Planck*, *Astron. Astrophys.* **641** (2020) A1, [[arXiv:1807.06205](#)].
- [26] **Planck** Collaboration, N. Aghanim et al., *Planck 2018 results. V. CMB power spectra and likelihoods*, *Astron. Astrophys.* **641** (2020) A5, [[arXiv:1907.12875](#)].
- [27] **Planck** Collaboration, N. Aghanim et al., *Planck 2018 results. VIII. Gravitational lensing*, *Astron. Astrophys.* **641** (2020) A8, [[arXiv:1807.06210](#)].
- [28] **DESI** Collaboration, M. Abdul Karim et al., *DESI DR2 results. I. Baryon acoustic oscillations from the Lyman alpha forest*, *Phys. Rev. D* **112** (2025), no. 8 083514, [[arXiv:2503.14739](#)].

- [29] D. Brout et al., *The Pantheon+ Analysis: Cosmological Constraints*, *Astrophys. J.* **938** (2022), no. 2 110, [[arXiv:2202.04077](https://arxiv.org/abs/2202.04077)].
- [30] A. G. Riess et al., *A Comprehensive Measurement of the Local Value of the Hubble Constant with $1 \text{ km s}^{-1} \text{ Mpc}^{-1}$ Uncertainty from the Hubble Space Telescope and the SH0ES Team*, *Astrophys. J. Lett.* **934** (2022), no. 1 L7, [[arXiv:2112.04510](https://arxiv.org/abs/2112.04510)].
- [31] D. Rubin et al., *Union Through UNITY: Cosmology with 2,000 SNe Using a Unified Bayesian Framework*, *Astrophys. J.* **986** (2025), no. 2 231, [[arXiv:2311.12098](https://arxiv.org/abs/2311.12098)].
- [32] **DES** Collaboration, T. M. C. Abbott et al., *The Dark Energy Survey: Cosmology Results with ~ 1500 New High-redshift Type Ia Supernovae Using the Full 5 yr Data Set*, *Astrophys. J. Lett.* **973** (2024), no. 1 L14, [[arXiv:2401.02929](https://arxiv.org/abs/2401.02929)].
- [33] J. Torrado and A. Lewis, *Cobaya: Code for Bayesian Analysis of hierarchical physical models*, *JCAP* **05** (2021) 057, [[arXiv:2005.05290](https://arxiv.org/abs/2005.05290)].
- [34] A. Lewis and S. Bridle, *Cosmological parameters from CMB and other data: A Monte Carlo approach*, *Phys. Rev. D* **66** (2002) 103511, [[astro-ph/0205436](https://arxiv.org/abs/astro-ph/0205436)].
- [35] A. Lewis, *Efficient sampling of fast and slow cosmological parameters*, *Phys. Rev. D* **87** (2013), no. 10 103529, [[arXiv:1304.4473](https://arxiv.org/abs/1304.4473)].
- [36] R. M. Neal, *Taking Bigger Metropolis Steps by Dragging Fast Variables*, [math/0502099](https://arxiv.org/abs/math/0502099).
- [37] A. Gelman and D. B. Rubin, *Inference from Iterative Simulation Using Multiple Sequences*, *Statist. Sci.* **7** (1992) 457–472.
- [38] A. Lewis, *GetDist: a Python package for analysing Monte Carlo samples*, *JCAP* **08** (2025) 025, [[arXiv:1910.13970](https://arxiv.org/abs/1910.13970)].
- [39] A. H. Wright et al., *KiDS-Legacy: Cosmological constraints from cosmic shear with the complete Kilo-Degree Survey*, *Astron. Astrophys.* **703** (2025) A158, [[arXiv:2503.19441](https://arxiv.org/abs/2503.19441)].
- [40] H. Akaike, *A new look at the statistical model identification*, *IEEE Trans. Automatic Control* **19** (1974), no. 6 716–723.